

---

# A SCALABLE BAYESIAN SPATIOTEMPORAL MODEL FOR WATER LEVEL PREDICTIONS USING A NEAREST NEIGHBOR GAUSSIAN PROCESS APPROACH

---

**Victor Hugo Nagahama**

Hamilton Institute  
Maynooth University  
victor.nagahama.2022@mumail.ie

**James Sweeney**

Department of Mathematics and Statistics  
University of Limerick  
james.a.sweeney@ul.ie

**Niamh Cahill**

Department of Mathematics and Statistics  
Maynooth University  
niamh.cahill@mu.ie

December 11, 2024

## ABSTRACT

Obtaining accurate water level predictions are essential for water resource management and implementing flood mitigation strategies. Several data-driven models can be found in the literature. However, there has been limited research with regard to addressing the challenges posed by large spatio-temporally referenced hydrological datasets, in particular, the challenges of maintaining predictive performance and uncertainty quantification. Gaussian Processes (GPs) are commonly used to capture complex space-time interactions. However, GPs are computationally expensive and suffer from poor scaling as the number of locations increases due to required covariance matrix inversions. To overcome the computational bottleneck, the Nearest Neighbor Gaussian Process (NNGP) introduces a sparse precision matrix providing scalability without having to make inferential compromises. In this work we introduce an innovative model in the hydrology field, specifically designed to handle large datasets consisting of a large number of spatial points across multiple hydrological basins, with daily observations over an extended period. In this work, we investigate the application of a Bayesian spatiotemporal NNGP model to a rich dataset of daily water levels of rivers located in Ireland. The dataset comprises a network of 301 stations situated in various basins across Ireland, measured over a period of 90 days. The proposed approach allows for prediction of water levels at future time points, as well as the prediction of water levels at unobserved locations through spatial interpolation, while maintaining the benefits of the Bayesian approach, such as uncertainty propagation and quantification. Our findings demonstrate that the proposed model outperforms competing approaches in terms of accuracy and precision. When compared to single-basin approaches in the field of hydrology, our model achieves scalability and the ability to extend predictions across a broader range of river basins with minimal trade-off in predictive performance.

## 1 Introduction

In Ireland, rivers serve as a primary source of freshwater, providing drinking water to households, supporting industrial processes, and sustaining agriculture. The monitoring of water levels enables authorities to predict and manage water availability, especially during dry periods, as low levels can lead to water shortages, while high levels may require preventative measures to avert flooding and contamination in terms of sewage. Accurate predictions of river water levels are essential for effective water resource management and flood mitigation strategies.

---

Ireland's climate contributes to significant fluctuations in water levels with heavy precipitation in autumn and winter particularly. At these times there is heightened flood risk in many areas. Flood events lead to both direct economic losses, such as damage to infrastructure and property, and indirect losses through disruptions to economic activity. Between 1996 and 2015, the global economic losses from flooding were estimated at 597 billion USD (Willner et al., 2018). Accurate water level prediction is therefore increasingly important in Ireland, given the rising demand for water across industrial and domestic sectors and the growing frequency of flood events (Charlton et al., 2006). Additionally, the intensification of precipitation patterns as a consequence of climate change increases the risks of flooding (Murphy et al., 2023). This highlights the critical need for accurate inputs to flood mapping models in order to protect communities and support resilient infrastructure planning.

In the hydrology field, water level recordings have been traditionally collected through physical sensors strategically placed along the river stream, creating a spatial network of monitoring stations that collect data over time. The main challenge of making water level predictions is capturing the intrinsic spatiotemporal dynamics of river systems while accounting for related influencing factors. For instance, precipitation events increase water levels while evaporation has the opposite effect, contributing to water level reductions. Indeed, empirical studies have demonstrated that precipitation in the preceding day is the most significant factor for water level increases as precipitation makes its way through the soil or across non absorptive surfaces (Kenda et al., 2020; Ahmed et al., 2022). Another challenge inherent to the task of predicting water levels is the quality of the data. Physical sensors are prone to malfunctions, which can result in missing or unreliable measurements that introduce biases into the data. This has the potential to compromise predictive model accuracy and introduces additional complexity to the prediction task, since data-driven models often require effective pre-processing to handle such issues prior to being able to generate predictions.

In the literature, two main approaches are employed for predicting water levels: hydrological simulations and/or data-driven models. The former uses physical models to simulate the water level dynamics through several obligatory inputs, such as soil and land-use related parameters, leaf area index and snow melt and frost parameters. However, these methods are often computationally costly, especially for large simulations and rely on assumptions of the input parameters derived from published literature (van der Knijff et al., 2010). For the latter, many data-driven methods have been applied to predict water levels within a space and time context using machine learning and statistical techniques. Pan et al. (2020) applied a convolutional neural network to predict daily water levels over an extended period (30 years) but only considered four water stations. More recently, Pagendam et al. (2023) tackled a large dataset consisting of weekly observations of groundwater depth using a deep neural network with two sub-architectures highlighting the advances of computational efficient methods. However, these machine learning models are less transparent, more difficult to interpret than statistical models and uncertainty quantification for model predictions are challenging.

Space-time kriging has been widely applied to predict water levels under the frequentest (non-Bayesian) paradigm but can suffer from poor scaling as the number of locations increases (Varouchakis et al., 2022; Ruybal et al., 2019; Hoogland et al., 2010; J nez-Ferreira and Herrera, 2013; Kazemi et al., 2021). The Gaussian Process (GP) model is frequently used in the hydrological literature since it is capable of modeling complex space-time dependent covariance structures while providing a flexible approach for approximating smooth functions. Additionally, the approach has been widely studied under the frequentist and Bayesian paradigm. There is a strong connection between GPs and regression kriging, and these can be viewed as interchangeable in some scenarios. However, Varouchakis and Hristopulos (2019) showed that GPs demonstrate superior performance when compared to kriging. In general, both GP and kriging approaches are susceptible to computational limitations when applied to large dataset due to the inversions of covariance matrices.

The seminal paper of Vecchia (1988) introduced an approximation for the GP that alleviates this computational limitation. As a result, the modified GP is scalable for larger datasets while keeping the benefits of a GP. Later, Datta et al. (2016a) used this concept to propose the Nearest Neighbor Gaussian Process (NNGP) model and showed that this approximation is also a valid spatial process for the whole spatial domain without compromising inferential accuracy. More recently, the NNGP approach has achieved the state of the art in predictions at the second KAUST spatial statistics competition which compared different methodologies for spatial and spatiotemporal process (Abdulah et al., 2022). The application of NNGP approach to the field of climate science is a topic already addressed in the existing literature. For instance, (Datta et al., 2016b) investigated its predictive capabilities for a particulate matter air quality dataset. Mastrantonio et al. (2019) proposed a hierarchical multivariate NNGP model for predicting monthly precipitation, minimum and maximum temperatures. However, there is little to no consideration in the literature of its application to hydrological datasets.

In the field of hydrology, where missing values are a common occurrence, non-Bayesian approaches, such as those discussed above, have the disadvantage of requiring the use of an auxiliary model to address the missingness of data. In contrast, Bayesian approaches offer a natural solution for imputation through the specification of prior distributions. Molinos et al. (2015) proposed a Bayesian harmonic regression model to predict monthly water levels in Irish lakes considering an extended period (1974 - 2012) while accounting for seasonal effects. While this study provided

insights into long-term water level trends, it analysed recordings from only 28 spatial locations. Related to water levels, Santos-Fernandez et al. (2022) proposed various Bayesian vector autoregressive (VAR) models to predict daily water temperature in rivers, considering covariance functions depending on stream networks and Euclidean distances. However, despite the innovation introduced by the authors, computational issues arise again as the method scales poorly for a large number of spatial points.

Despite the development of spatiotemporal models in the field of hydrology, there have been few successful studies addressing the challenge of predicting water levels across a dense network of monitoring stations with extensive temporal records, all while maintaining computational efficiency and model performance. This task remains complex, as it requires a model capable of simultaneously overcoming the computational limitations, capturing the space-time dependencies and accounting for prediction uncertainty and data gaps. In order to address this challenge, we propose a Bayesian spatiotemporal NNGP model to predict daily water levels considering a large number of stations located in Ireland recorded over an extended period. The dataset consists of a dense network of 301 stations each measured over 90 days. The model incorporates the past-day precipitation as a predictor with an additive spatiotemporal effect following a first-order autoregressive process. The proposed approach allows for predicting both monitored stations in a future day and predicting unobserved locations through the use of interpolation.

The remainder of the paper is structured as follows. In Section 2 we describe the water level and precipitation dataset in Ireland. In Section 3 the NNGP definition and detailed explanation of the proposed spatiotemporal NNGP model is presented. In Section 4, we present the strategy and metrics used to assess model performance, followed by the results of applying the model to both synthetic and real-world water level data. Following that, in Section 5 we compare our proposed model with alternative approaches documented in the literature. In Section 6 the limitations of this study are discussed. Finally, the Section 7 concludes the paper with a summary of findings and suggestions for future research.

## 2 Water level and precipitation records in Ireland

The Office of Public Works (OPW) collects water level and additional variables in a daily frequency for an extensive hydrometric network of 380 monitoring stations located on rivers, lakes and tidal locations throughout the Republic of Ireland. The data is accessible via the Application Programming Interface (API) which can be accessed at <https://waterlevel.ie/> (OPW, 2021). For this study, we selected only those stations located on rivers and extracted the water level recordings (in meters) for the period between 03/01/2022 and 02/04/2022. To ensure the reliability of the records, stations with more than 30% of missing data were ignored, resulting in 301 stations. Given the substantial variability in the average water level across rivers, we subtracted the water level recordings of each station by their respective means, resulting in a zero-centered distribution (see Figure 1). The distances between locations were calculated using the great circle distance to account for the curvature of the earth, thus enhancing precision and ensuring a representation in kilometres.

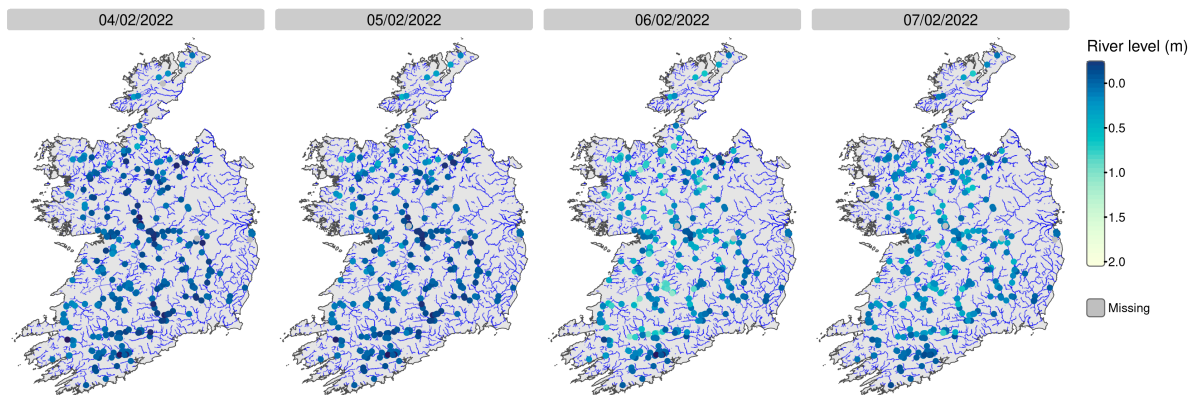


Figure 1: Zero-centered water levels (in meters) observed at stations across Ireland between 4 February 2022 and 7 February 2022.

The Irish Meteorological Service, Met Éireann provides forecasting and access to historical data on several weather variables, including 24 hours precipitation accumulation, temperature, wind speed, soil moisture and potential evapotranspiration. We extracted the precipitation variable from the available weather stations, covering

---

the same one-year period as the water level data. The data retrieval was facilitated using the API available at <https://marie.ie/repo/met-eireann-api/> (Marie, 2023).

The observed precipitation did not align with the coordinates of river stations (see Figure 2). To address this spatial misalignment, the Inverse Distance Weighting (IDW) interpolation was applied to estimate the rainfall at each river station. The IDW is a deterministic interpolation method where the estimated values are calculated as weighted averages of observed values, with the weights being inversely proportional to the distance between each observed point and the new point. The methodology has been demonstrated to be effective for interpolating precipitation data, as evidenced by (Chen and Liu, 2012).

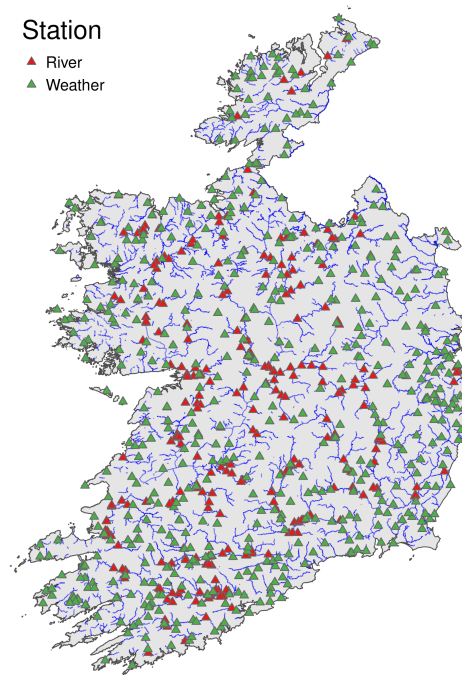


Figure 2: Map of Ireland illustrating the spatial misalignment between river (red) and hydroclimate stations (green).

In order to address the heavily right-skewed distribution of precipitation and strengthen its correlation with water level, we applied the square root transformation. Furthermore, in recognition of the delayed impact of precipitation on water level, we considered the precipitation from the previous day (lagged precipitation) as a predictor (see Figure 3). For clarity, we will refer to this transformed and lagged variable as precipitation throughout the analysis.

The left panel in Figure 4 illustrates the temporal evolution of water level across all stations throughout the study period. The figure reveals a general pattern among the majority of the stations with peak records occurring in February. The accompanying spatiotemporal semivariogram (right panel in Figure 4) provides further support for the trend pattern observed among the stations. The semivariance rapidly increases with distance and then flattens out, indicating a "sill" where the spatial correlation diminishes. However, the semivariance persists consistently over time, suggesting that while spatial proximity significantly influences water levels until a distance is reached, the temporal dynamics exhibit a long-lasting effect. The stations following different patterns to this may be attributed to site-specific influences or unreliable measurements.

When inspecting simultaneously the water level and precipitation records, we see high water levels in February as a result of intense precipitation (Figure 5). In Ireland, the wet season typically occurs in February and March. Despite March being classified as a wet month (the precipitation records at the beginning of the month can be comparable to February), the distribution of water levels resembles the observed levels in January. This suggests that factors beyond precipitation are likely influencing water level variations.

The impact of water level drivers beyond precipitation is clearly demonstrated when examining the fluctuations in water levels across stations over time (Figure 6). However, precipitation peaks consistently occur in late February and early March, water levels show significant variation in how they respond to these peaks across different stations. This pattern

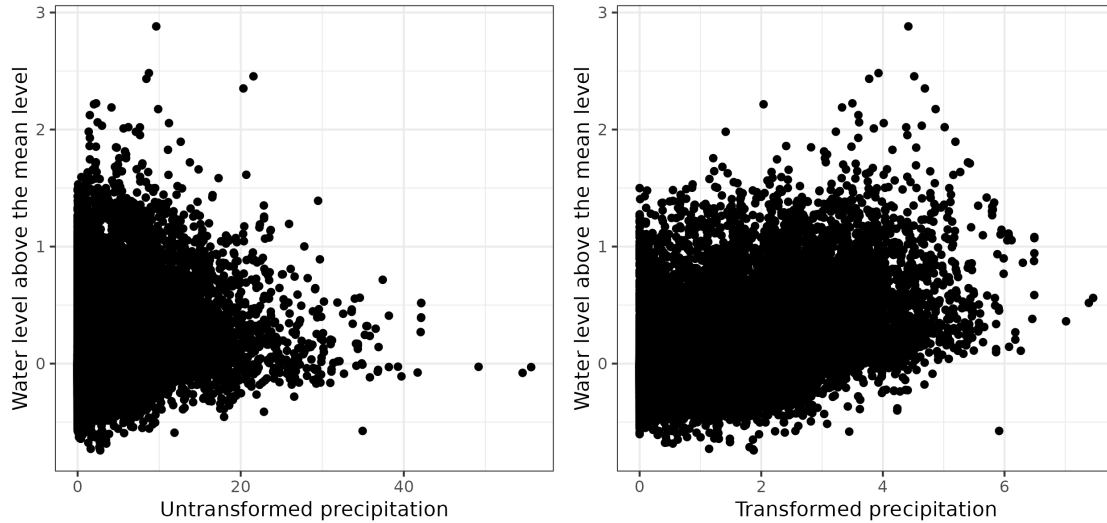


Figure 3: Left: precipitation before (square root and lag) transformation versus zero-centered water level. Right: precipitation after the transformation versus zero-centered water level.

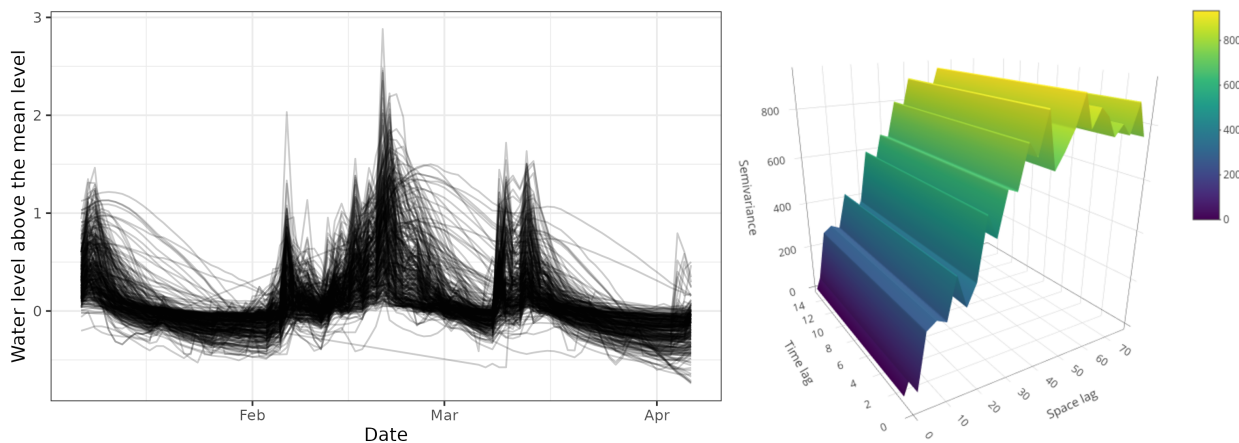


Figure 4: Left: temporal evolution of water level. Right: empirical spatiotemporal semivariogram for the considered monitoring stations.

indicates that additional hydroclimate factors such as soil saturation and evapotranspiration rates may be shaping the observed water level dynamics alongside precipitation. Furthermore, stations with similar water level variations may be situated in close proximity to one another, indicating the presence of a spatial correlation (as previously highlighted in the right panel in Figure 4).

### 3 Methodology

The proposed model is inspired by a study on Australian river water temperatures by Santos-Fernandez et al. (2022), which was selected due to its suitability for addressing the challenges posed by long-term spatiotemporal data (42 spatial locations measured over 87 days), a time dimension similar to the current study. The authors proposed a Bayesian spatiotemporal model for predicting water temperature where the temporal correlation is captured through an autoregressive parameter and the spatial dependence along the river network is modeled using a Gaussian Process (GP) that incorporates stream distance. In contrast, our study deals with a significantly larger dataset comprising 301 spatial locations compared to their 42. This substantial increase in spatial points makes the use of a conventional GP computationally impractical due to the inversion of a large spatial covariance matrix. In order to address the computational limitation, we employed the Nearest Neighbor Gaussian Process (NNGP), a scalable alternative that

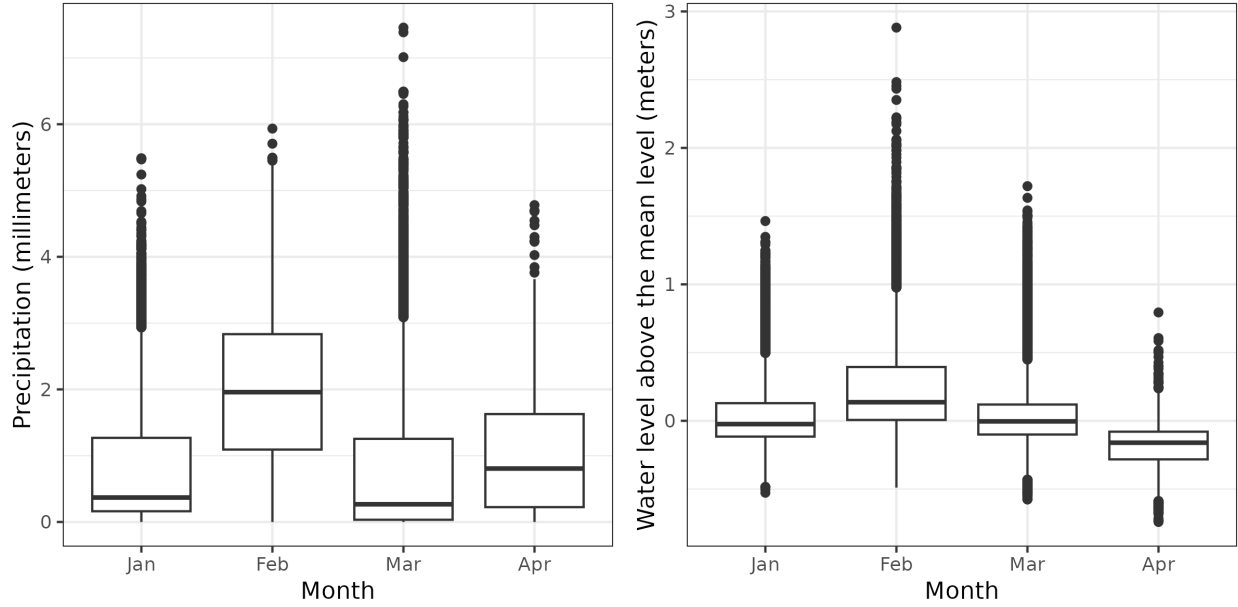


Figure 5: Left: boxplot of water level above the mean level (meters). Right: precipitation (millimetres) by month.

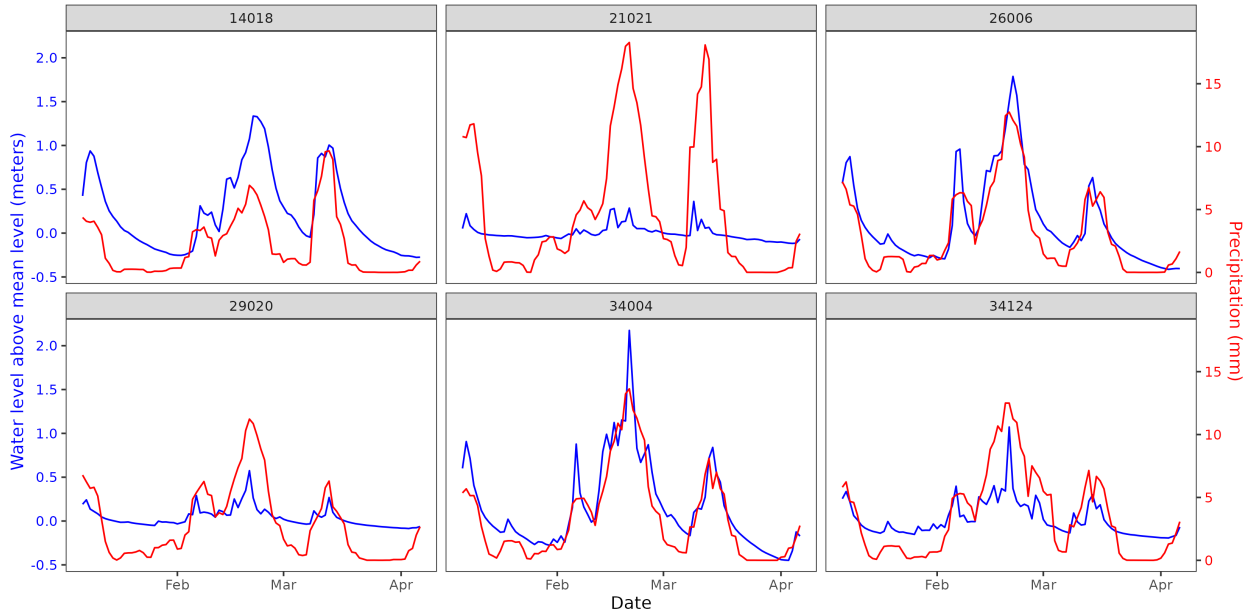


Figure 6: Water level above the mean level (meters) and precipitation (millimetres) at six river monitoring stations.

effectively approximates the GP while preserving spatial dependencies. First, we present the concept of NNGP in Section 3.1. Subsequently, we define the proposed spatiotemporal model in Section 3.2.

### 3.1 Nearest Neighbor Gaussian Process

Let  $\mathbf{s} = \{s_1, \dots, s_n\}$  be the set of spatial locations in the spatial domain  $\mathcal{S} \subset \mathbb{R}^d$  and consider a pure spatial process following a zero-centered GP with covariance matrix  $\Sigma = \Sigma(\cdot, \cdot)$ , denoted as  $\mathbf{w} \sim GP(\mathbf{0}, \Sigma)$ . The process can be

expressed as the product of conditional normal distributions

$$p(\mathbf{w}) = p(w(\mathbf{s}_1)) \prod_{i=2}^n p(w(\mathbf{s}_i) \mid w(\mathbf{s}_{i-1}), \dots, w(\mathbf{s}_1)). \quad (1)$$

In a setting with a substantial number of spatial locations, some elements within the conditional set provide a superfluous contribution, in such a manner that their exclusion results in minimal loss of information. The underlying idea of the NNGP is to substitute each extensive conditional set by a subset (smaller set) containing at most  $m$  nearest neighbors (Vecchia, 1988). Formally, let  $N(\mathbf{s}_i)$  be the subset of  $m$  nearest neighbors of location  $\mathbf{s}_i$ , that is,  $N(\mathbf{s}_i) \subset \{\mathbf{s}_1, \dots, \mathbf{s}_{i-1}\}$ . We have an approximation for Equation 1, known as the Nearest Neighbor Gaussian Process (NNGP) denoted by  $\tilde{\mathbf{w}} \sim \text{NNGP}(\mathbf{0}, \tilde{\Sigma})$

$$p(\mathbf{w}) \approx p(\tilde{\mathbf{w}}) = p(w(\mathbf{s}_1)) \prod_{i=2}^n p(w(\mathbf{s}_i) \mid \mathbf{w}(N(\mathbf{s}_i))). \quad (2)$$

As demonstrated by Datta et al. (2016a) the stated approximation is a valid multivariate normal distribution and also is a valid spatial process over  $\mathcal{S}$ . Hence the predictions are close to the GP model and the NNGP kriging recovers the true spatial process. Defining the neighbor set  $N(\mathbf{s}_i)$  requires imposing an order on locations, such that any given order generates a valid joint distribution. We followed the approach as suggested by Datta et al. (2016a), ordering according to one of the spatial coordinates, providing a convenient and effective solution. Indeed, we ordered the spatial locations by the latitude coordinate.

From probability theory of the multivariate Normal distribution, each of the conditional densities in Equation 2 is also normally distributed with parameters

$$\mathbb{E}[w(\mathbf{s}_i) \mid \mathbf{w}(N(\mathbf{s}_i))] = \mathbf{a}_i \mathbf{w}(N(\mathbf{s}_i)) \quad (3)$$

$$\mathbb{V}[w(\mathbf{s}_i) \mid \mathbf{w}(N(\mathbf{s}_i))] = d_i, \quad (4)$$

where  $\mathbf{a}_i = \Sigma(\mathbf{s}_i, N(\mathbf{s}_i))\Sigma(N(\mathbf{s}_i), N(\mathbf{s}_i))^{-1}$  and  $d_i = \Sigma(\mathbf{s}_i, \mathbf{s}_i) - \mathbf{a}_i \Sigma(\mathbf{s}_i, N(\mathbf{s}_i))^T$ .

The presented NNGP was formulated as a zero-centered distribution but it is trivial to shift the mean to accommodate a non-zero centered process. Furthermore, the process can be simply extended to a space-time setting, with the incorporation of a separable spatiotemporal covariance model, as detailed in Section 3.2.

### 3.2 The spatiotemporal model

Let  $\mathbf{y}_t$  be the vector of water level measurements for all locations at time  $t = 1, \dots, T$  and the stacked vector  $[\mathbf{y}_1, \mathbf{y}_2, \dots, \mathbf{y}_T]$  representing the multivariate distribution for all locations and time points. We propose a model based on the conditional distributions

$$[\mathbf{y}_1, \mathbf{y}_2, \dots, \mathbf{y}_T] = p(\mathbf{y}_1 \mid \mathbf{X}_1, \boldsymbol{\theta}) \prod_{t=2}^T p(\mathbf{y}_t \mid \mathbf{y}_{t-1}, \mathbf{X}_t, \mathbf{X}_{t-1}, \boldsymbol{\theta}), \quad (5)$$

where  $\mathbf{X}_t$  is the design matrix of predictors at time  $t$ ,  $\boldsymbol{\theta}$  is the vector of parameters and  $\mathbf{y}_1$  is the distribution at time  $t = 1$ . For the following time points the distribution is given by

$$p(\mathbf{y}_t \mid \mathbf{y}_{t-1}, \mathbf{X}_t, \mathbf{X}_{t-1}, \boldsymbol{\theta}) \sim \mathcal{N}(\mathbf{y}_t; \boldsymbol{\mu}_t, \tilde{\Sigma} + \tau^2 \mathbf{I}), \quad (6)$$

where  $\tilde{\Sigma}$  is the exponential covariance matrix from a NNGP and  $\tau^2 \mathbf{I}$  is the matrix of errors. The mean parameter of the distribution is

$$\boldsymbol{\mu}_t = \mathbf{X}_t \boldsymbol{\beta} + \phi(\mathbf{y}_{t-1} - \mathbf{X}_{t-1} \boldsymbol{\beta}). \quad (7)$$

The model is second-order stationary following a multivariate normal distribution where the time process is an additive term in the mean parameter while the spatial process is included through the spatial covariance matrix. Indeed, the mean at the current time depends on the predictors and the response at the previous time point scaled by the autoregressive parameter  $|\phi| < 1$ . The model presented in Equation 6 exploits the benefits of the normal likelihood by integrating out the spatial process, resulting in what is known as the marginal model (Finley et al., 2019). Sampling from this formulation is preferable as it enhances stability by reducing the dimensionality of the parameter space. However, for prediction extrapolating the time dimension, the marginal model is not practical, as it requires the values of predictors

for all locations in a future time point. An equivalent formulation, referred to as the latent model, can be used in such cases. This latent model is explicitly expressed in terms of the spatial latent field, that is

$$\mathbf{y}_t = \mathbf{X}_t\boldsymbol{\beta} + \phi(\mathbf{y}_{t-1} - \mathbf{X}_{t-1}\boldsymbol{\beta}) + \tilde{\mathbf{w}}_t + \boldsymbol{\varepsilon}_t, \quad (8)$$

where  $\tilde{\mathbf{w}}_t \sim NNGP(\mathbf{0}, \tilde{\boldsymbol{\Sigma}})$  and  $\boldsymbol{\varepsilon}_t \sim \mathcal{N}(\mathbf{0}, \tau^2\mathbf{I})$ . As stated previously, the marginal model is more computationally efficient, therefore, we used that formulation for sampling from the posterior and for predictions purely in space. In contrast, the latent model (Equation 8) is used for making predictions that require extrapolation over time. Detailed explanations of the predictions are provided in Section 3.3.

Uninformative priors were assumed for the regression parameters,  $\mathcal{N}(0, 100)$ , whereas for the autoregressive parameter a non-informative prior was assigned,  $\phi \sim U(-1, 1)$ . For the variance parameters, we assumed conjugate priors,  $\sigma^2 \sim IG(2, 1)$ , and a tighter prior for the error variance to ensure the identifiability of the model,  $\tau^2 \sim IG(2, 0.1)$ . The length-scale parameter was assumed as  $l \sim U(0.1, 300)$  that corresponds to an effective range of  $[0.3, 900]$  km. Finally, the number of nearest neighbors was set to 10, as this value produced satisfactory results when tested on a synthetic dataset used to validate the approach, see the results in Section 4.1). This choice aligns with findings by Datta et al. (2016a), who demonstrated that modest values of  $m < 20$  offers balance between computational efficiency and predictive accuracy in NNGP models.

A full Bayesian inference approach was employed to naturally handle missing values and provide thorough quantification of uncertainty. The model was implemented in Stan using Markov Chain Monte Carlo (MCMC) sampling via No-U-Turn Sampler (NUTS). In order to facilitate the interface with Stan, the `cmdstanr` package in R was used (Gabry et al., 2024). The implementation efficiently completed 500 iterations across 4 chains in approximately 17 minutes. The code used for model implementation is available in this Github repository. All scripts and instructions necessary to reproduce the results are provided.

### 3.3 Spatiotemporal prediction

The proposed spatiotemporal model allows predictions across both time and space, with the extrapolations being made along each of the dimensions either individually or simultaneously. First, we present the approach for predicting over space and time at an unobserved location. Following that, we present the method for predicting future values at locations with historical observations. Here, we introduce the notation for the predictive scenarios. Let  $[\mathbf{y}_t] = [\mathbf{y}_1, \dots, \mathbf{y}_t]$  be the vector of water level measurements for all locations until the observed time  $t = 1, \dots, T$ . Consider an observed location  $\mathbf{s}_{obs}$  where we want to make predictions at a future time point. Additionally, an unobserved (new) location  $\mathbf{s}_{new}$  where we want to predict the water level either for a past of future time point. The three prediction scenarios that we implemented are detailed below.

#### 3.3.1 Unobserved (new) location at a past time point

Given an unobserved (new) location denoted by  $\mathbf{s}_{new}$ , we want to obtain the conditional distribution  $p(y_t(\mathbf{s}_{new}) \mid [\mathbf{y}_t])$ , for any past time point  $t = 1, \dots, T$ . This can be derived from the joint distribution of the unobserved location and the observed data at the given time point. This derivation is based on the marginal model (Equation 6) by conditioning on the observed data to obtain predictions for unobserved locations. The joint distribution is given by

$$\begin{bmatrix} y_t(\mathbf{s}_{new}) \mid y_{t-1}(\mathbf{s}_{new}) \\ \mathbf{y}_t(N(\mathbf{s}_{new})) \mid \mathbf{y}_{t-1}(N(\mathbf{s}_{new})) \end{bmatrix} \sim \mathcal{N} \left( \begin{bmatrix} \mu_t(\mathbf{s}_{new}) \\ \boldsymbol{\mu}_t(N(\mathbf{s}_{new})) \end{bmatrix}, \begin{bmatrix} \sigma^2 & \Sigma(\mathbf{s}_{new}, N(\mathbf{s}_{new}))^T \\ \Sigma(\mathbf{s}_{new}, N(\mathbf{s}_{new})) & \Sigma_N \end{bmatrix} \right),$$

where  $\Sigma_N = \Sigma(N(\mathbf{s}_{new}), N(\mathbf{s}_{new})) + \tau^2\mathbf{I}$ . Notice that the distribution can only be determined by using the preceding distribution of  $y_t(\mathbf{s}_{new})$  until the desired time point time  $t$ . From probability theory of the multivariate Normal distribution the conditional distribution is

$$\begin{aligned} y_t(\mathbf{s}_{new}) \mid y_{t-1}(\mathbf{s}_{new}), \mathbf{y}_t, \mathbf{y}_{t-1} &\sim \mathcal{N}(\alpha, \gamma) \\ \alpha &= \mu_t(\mathbf{s}_{new}) + \Sigma(\mathbf{s}_{new}, N(\mathbf{s}_{new}))(\sigma^2)^{-1}(\mathbf{y}_t(N(\mathbf{s}_{new})) - \boldsymbol{\mu}_t(N(\mathbf{s}_{new}))) \\ \gamma &= \sigma^2 - \Sigma(\mathbf{s}_{new}, N(\mathbf{s}_{new}))\Sigma_N^{-1}\Sigma(\mathbf{s}_{new}, N(\mathbf{s}_{new}))^T. \end{aligned}$$

#### 3.3.2 Unobserved (new) location at a future time point

In order to obtain samples of the conditional distribution of  $p(y_t(\mathbf{s}_{new}) \mid [\mathbf{y}_t])$  for a future time point  $t > T$ , we have to make use of the latent model. This model is necessary because, at future time points, predictors at all other locations

are usually unknown, a requirement for the marginal model. However, for the latent model, only the predictors at the target location are needed, though it requires obtaining samples from the spatial latent field specifically for that location, denoted as  $\tilde{w}_t(\mathbf{s}_{new})$ . We proceed by sampling by composition, first drawing from the predictive distribution of  $\tilde{w}_t(\mathbf{s}_{new})$  and then using the latent model (Equation 8) to draw samples from  $y_t(\mathbf{s}_{new})$ . The first step is done by kriging the spatial latent field at the given time point. The joint distribution is

$$\begin{bmatrix} \tilde{w}_t(\mathbf{s}_{new}) \\ \tilde{\mathbf{w}}_t(N(\mathbf{s}_{new})) \end{bmatrix} \sim \mathcal{N} \left( \mathbf{0}, \begin{bmatrix} \sigma^2 & \Sigma(\mathbf{s}_{new}, N(\mathbf{s}_{new}))^T \\ \Sigma(\mathbf{s}_{new}, N(\mathbf{s}_{new})) & \tilde{\Sigma}_N \end{bmatrix} \right),$$

where  $\tilde{\Sigma}_N = \Sigma(N(\mathbf{s}_{new}), N(\mathbf{s}_{new}))$ . Therefore the predictive distribution of  $\tilde{w}_t(\mathbf{s}_{new})$  has similar form of Equations 3 and 4.

### 3.3.3 Observed location at a future time point

Given a observed location denoted by  $\mathbf{s}_{obs}$ , we want to obtain the conditional distribution of  $p(y_t(\mathbf{s}_{obs}) | [\mathbf{y}_t])$ , for a future time point  $t > T$ . Similar for prediction of unobserved (new) locations at a future time point, this involves sampling from the posterior latent field at the future time point before drawing samples from the distribution of interest. However, the location of interest is known, therefore, kriging is not required here. This is because  $\tilde{w}_t(\mathbf{s}_{obs})$  is directly part of the spatial latent field  $\tilde{\mathbf{w}}_t$  eliminating the need for spatial interpolation at the observed location.

## 4 Application

This section presents an analysis of a synthetic dataset using the proposed model, followed by its application to the Irish water level dataset. The objective of the application to the synthetic data is to evaluate the model performance under controlled conditions, and assess its capability for imputing missing values.

In terms of performance, the goal is to make predictions at locations where there is no data available, as well as to forecast future observations at sites with existing data. In order to evaluate the model performance in both scenarios, an out-of-sample (OOS) evaluation was conducted, splitting the data into two subsets: training and validation. Specifically, the validation dataset consisted of two components: (1) a random selection of stations that included all available time points, and (2) the reservation of the last three days of observations for the remaining stations. The illustrative diagram in Figure 7 represents the data splitting strategy for a total of 20 stations.

The Section 4.1 first presents the data generation procedure with missing values and the application of the mentioned splitting setup. Subsequently, it outlines the results obtained by the proposed model. The Section 4.2 presents the validation results of the proposed model for the water level dataset, where 20 stations were randomly selected for testing. This left a training set consisting of 281 stations, each measured over a period of 85 days, resulting in a total of 27,090 observations.

### 4.1 Synthetic dataset

We simulated a spatiotemporal dataset composed of 100 spatial locations within a unit square domain, each measured for 20 days, in a total of  $100 \times 20 = 2,000$  observations. First we simulated the spatial locations in a unit square. Following that, the spatial covariance matrix was computed using the exponential function with parameters  $\sigma^2 = 1$  and  $l = 0.3$ . The response variable was then simulated sequentially from  $t = 1$  onward, using Equation 6. The mean function (Equation 7) assumed regression coefficients  $\beta = [1, 3]$  and  $\phi = 0.9$ . The parameter values were selected in a manner that ensured the temporal correlation resulted in a long-lasting effect while simultaneously preventing the spatial parameters from being overly smoothed or localised. Finally, the space-time process was fully specified adding the error variance ( $\tau^2 = 0.1$ ) into the spatial covariance. We can summarise the generation of the synthetic dataset as

$$\begin{cases} \mathbf{x}_t \sim \mathcal{N}(\mathbf{0}, \mathbf{I}), & t = 1, \dots, 20 \\ \mathbf{s} = \{\mathbf{s}_1, \dots, \mathbf{s}_{100}\} \text{ where } \mathbf{s}_i = (u_1, u_2) \text{ and } u_1, u_2 \sim Unif(0, 1), & i = 1, \dots, 100 \\ \Sigma = \Sigma(\mathbf{s}_i, \mathbf{s}_j) = \exp\left(-\frac{|\mathbf{s}_i - \mathbf{s}_j|}{0.3}\right) + 0.1^2 \mathbf{I} \\ \mathbf{y}_1 \sim \mathcal{N}(1 + 3\mathbf{x}_1, \Sigma/(1 - \phi^2)) \\ \boldsymbol{\mu}_t = 1 + 3\mathbf{x}_t + 0.9 \times (\mathbf{y}_{t-1} - (1 + 3\mathbf{x}_t)), & t > 1 \\ \mathbf{y}_t \sim \mathcal{N}(\boldsymbol{\mu}_t, \Sigma), & t > 1. \end{cases}$$

In order to assess the imputation capability of the model, 10% of the simulated observations were set as missing. While, for prediction performance, we follow the same setup as presented in Figure 7 but using 10 spatial locations as



Figure 7: Illustrative diagram of training and validation dataset for out-of-sample evaluation. Each tile represents to a daily observation and coloured according to the data subset.

unobserved locations and leaving out the last day of the remaining observations for validation. The priors for the model were chosen as described in Section 3.2, with an adjustment made for the length-scale parameter to accommodate the spatial distances within the context of this synthetic data. In order to ensure an appropriate prior distribution in a unit square domain, the length-scale parameter was specified as  $l \sim U(0.1, 1)$ . Additionally, the number of nearest neighbors for the NNGP prior was set to 10 to balance computational efficiency and spatial accuracy in the spatial latent field estimation.

Table 1 shows the posterior estimates for the synthetic data. The model successfully produces parameter estimates close to the true parameter values, with the 95% credible interval (CI) capturing all the parameter values, with the exception of the variance parameter. This indicates strong overall model performance in parameter estimation, though minor limitations in estimating the variance of the latent spatial field.

The model demonstrates accurate predictions in both scenarios: (1) predicting the values at previously observed locations for a future day, and (2) estimating the values for unobserved locations on days when other monitoring stations have recorded data. As illustrated in Figure 8, the posterior mean closely aligns the true values with the 95% prediction intervals successfully encompassing 99% of the true values. In terms of imputation capabilities, the model demonstrated high accuracy in recovering the true missing values. As shown in Figure 9, the posterior mean aligns with the true values with a high degree of precision, in fact, the 95% prediction intervals successfully contain the true values for approximately 93% of the missing observations. These results indicate that the proposed model effectively addresses complex spatiotemporal prediction problems where predictions can be across both space and time. Furthermore, the model demonstrates robust performance in imputing missing observations based on the posterior predictive distribution, eliminating the need for an auxiliary imputation model.

Table 1: Posterior estimates of model parameters in the synthetic dataset and its true values.

Parameter	True value	Mean	Median	95% CI
$\beta_0$	1.00	0.58	0.58	(-0.11, 1.22)
$\beta_1$	3.00	2.99	2.99	(2.97, 3.01)
$\phi$	0.90	0.91	0.91	(0.89, 0.93)
$\sigma^2$	1.00	1.23	1.23	(1.08, 1.41)
$\tau^2$	0.10	0.07	0.07	(0.05, 0.10)
$l$	0.30	0.25	0.25	(0.21, 0.30)

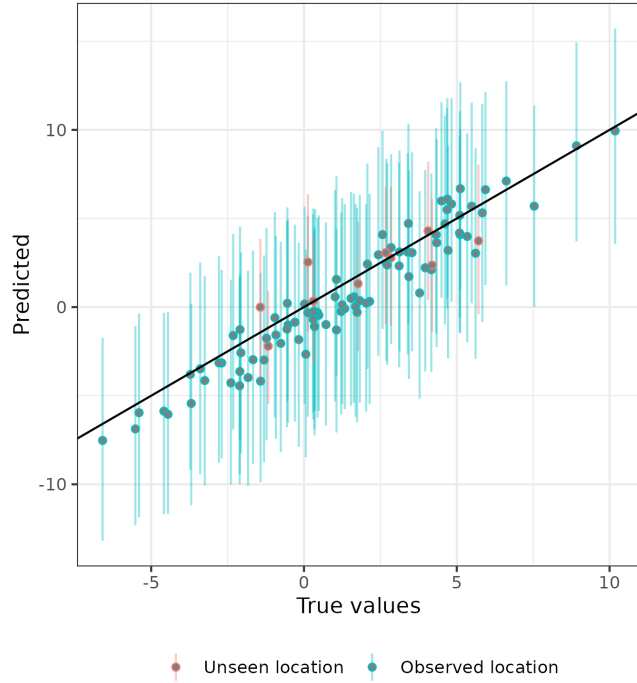


Figure 8: Predictive performance of the proposed model for the synthetic dataset considering prediction 1-day ahead under two different scenarios (unseen and observed locations). The dots represents the posterior mean while the vertical bars represent the 95% prediction interval.

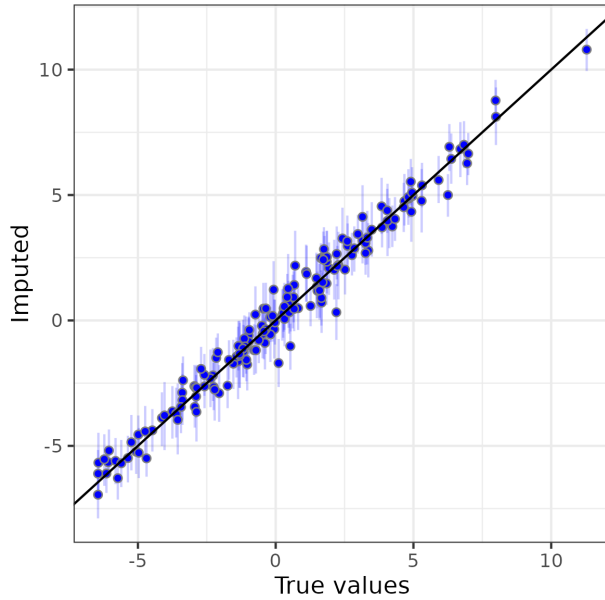


Figure 9: Imputation performance of the proposed model for the synthetic dataset. The dots represents the posterior mean while the vertical bars represent the 95% prediction interval.

#### 4.2 Water level dataset

Table 2 shows the posterior estimates for the water level dataset. The large value of  $\phi$  (0.89) highlights the high temporal dependence between the water level in consecutive days as our exploratory analysis previously indicated in Figure 4. In

other words, the water level in the future days is similar to the previous day if there is no large changes in precipitation. The posterior mean of the length-scale parameter is  $l = 24.53$  kilometers, which is a considerable range for the spatial decay. This range indicates that locations within approximately 25 kilometers of each other are correlated, which is consistent with the physical continuity of river networks and the gradual change in water levels over short distances. Furthermore, the proportion of variance that is captured by the spatial latent field -  $\sigma^2 / (\sigma^2 + \tau^2) \approx 0.76$  emphasising the importance of including the spatial component.

Table 2: Posterior estimates of model parameters in the water level dataset.

Parameter	Mean	Median	95% CI
$\beta_0$	0.01	0.01	(-0.02, 0.04)
$\beta_1$	0.05	0.05	(0.05, 0.99)
$\phi$	0.89	0.89	(0.88, 0.89)
$\sigma^2$	0.01	0.01	(0.01, 0.01)
$\tau^2$	0.003	0.003	(0.003, 0.004)
$l$	24.53	24.55	(23.22, 25.74)

After obtaining samples from the posterior distribution, they are used to predict the water levels at locations without available data and at future times. Figure 10 illustrates the comparison of the predicted and the true latent water level when predicting at one, two or three days in advance. The findings demonstrated that the model accurately predicts the true water level when predicting one and two days ahead. On the other hand, the prediction for three days ahead demonstrated inferior performance, with an underestimation of high water level records exceeding 0.4 meters. As expected, the prediction for an observed location on a future day exhibits superior accuracy and more narrow prediction intervals in comparison to sites without data (Table 3).

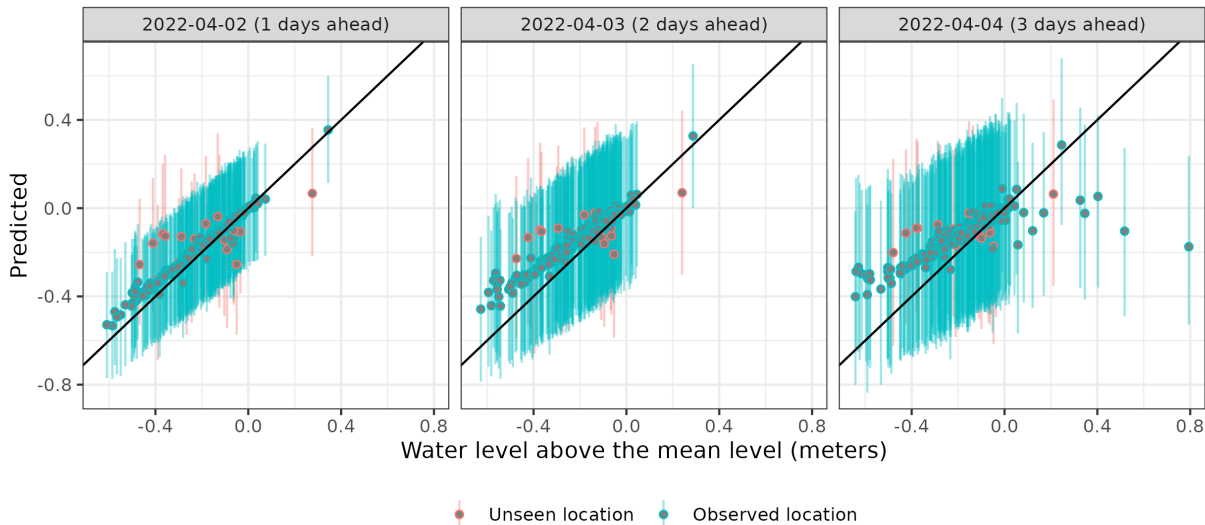


Figure 10: Predictive performance of the proposed model for the water level dataset considering predictions 1, 2 and 3-days ahead under two different scenarios (unseen and observed locations). The dots represents the posterior mean and while the vertical bars represent the 95% prediction interval.

Table 3: RMSE of OOS evaluation for prediction in 1, 2, 3-days ahead according to data availability.

Date	Observed locations	Unseen locations
02/04/2022 (1-day ahead)	0.039	0.141
03/04/2022 (2-day ahead)	0.081	0.155
04/04/2022 (3-day ahead)	0.129	0.160

Figure 11 depicts the predicted water level (after backtransformation) for 20 unobserved locations during the process of model fitting. At each observed time point, an interpolation was performed to estimate water levels at these unobserved

locations. For dates extending beyond the training dataset (02/04/2022 to 06/04/2022), the spatial latent field was first computed for the observed locations and subsequently interpolated in order to predict the water level at the unobserved locations, as outlined in Section 3.3. The limited information beyond 02/04/2022 is reflected in wider prediction intervals, indicating greater uncertainty in predictions.

In general, the model demonstrated the capacity to predict the water level for unobserved locations, including on a future day. However, for stations (18002, 18019, 25001 and 23030) the model struggles to accurately predict peak levels, though capturing well the general variation. Additionally, in some cases, the model overestimates the water level fluctuations (stations 14121 and 22009). These inconsistencies indicates that while the model exhibits satisfactory performance under typical circumstances, it may require additional refinement to handle site-specific characteristics.

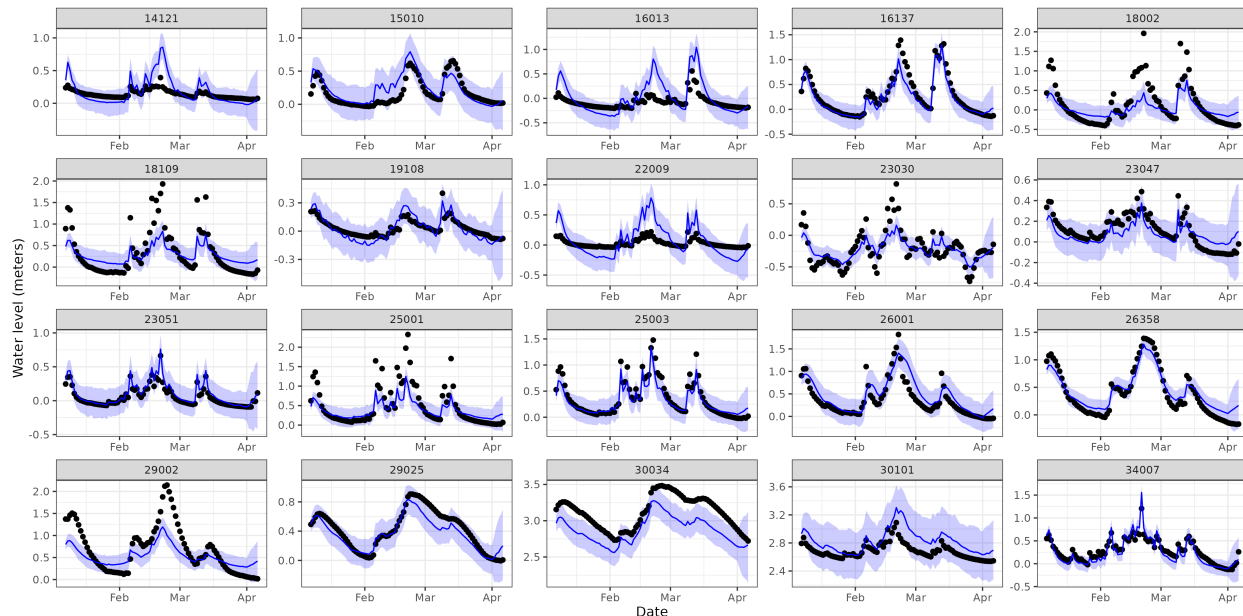


Figure 11: Predicted water level and its true values for 20 unobserved stations. The black dots represent the real values, while the blue line represents the posterior mean with the shaded area indicating the 95% prediction interval.

## 5 Model Comparison

Despite the model’s novelty in the hydrology field, we aim to compare its prediction performance and uncertainty quantification with other methodologies in the literature within two different setups: (1) comparison with a competitor model for large spatiotemporal datasets and (2) comparison with models focused on a single basin, which focus on river systems draining into a single large river, which is the approach commonly used by hydrologists. This dual comparison allows us to assess the model’s scalability and effectiveness across diverse hydrological contexts.

The selected criteria for assessing the predictive performance were Root Mean Square Error (RMSE) and Mean Absolute Error (MAE) on the out-of-sample data, which provide a measure of the accuracy of point predictions. In order to evaluate the uncertainty estimation and goodness of fit, the the prediction coverage at the 90% and 95% confidence levels was assessed. This metric measures the proportion of posterior intervals containing the true value, with a good model achieving coverage close to the confidence level. Additionally, the Continuous Ranked Probability Score (CRPS) was calculated, which penalises predictions when the prediction interval fails to capture the true value. Lower CRPS values indicate better performance (Gneiting and Raftery, 2007).

### 5.1 Comparison with a competitor model for large spatiotemporal data

For the first comparison, we selected the Gaussian Predictive Process (GPP) model. The model achieves scalability by defining a GP over a smaller set of locations, called knots, and then using kriging to predict the spatial effect at the observed locations (Sahu and Bakar, 2012). Formally, for a set of knot locations  $\mathbf{s}^* = \{\mathbf{s}_1^*, \dots, \mathbf{s}_m^*\}$  where  $m \ll n$ , the associated spatial process at time  $t$  is denoted by  $\mathbf{z}_t = \{z_t(\mathbf{s}_1^*), \dots, z_t(\mathbf{s}_m^*)\}$ . Therefore, the distribution

of observations at time  $t$  is given by

$$p(\mathbf{y}_t \mid \mathbf{X}_t, \mathbf{z}_t, \boldsymbol{\theta}) \sim \mathcal{N}(\mathbf{y}_t; \mathbf{X}_t \boldsymbol{\beta} + \tilde{\mathbf{w}}_t, \tau^2 \mathbf{I}), \quad (9)$$

where the spatial effect at observed locations can be approximated by  $\tilde{\mathbf{w}}_t = \mathbf{A} \boldsymbol{\Sigma}_z^{-1} \mathbf{z}_t$ . Also,  $\mathbf{A}$  denotes the covariance between the spatial effect at the observed locations and the knot location and  $\boldsymbol{\Sigma}_z$  is the covariance matrix of the spatial process  $\mathbf{z}_t$ . Moreover, to capture the temporal dependency, we assume the autoregressive model

$$\mathbf{z}_t = \rho \mathbf{z}_{t-1} + \boldsymbol{\xi}_t, \quad \boldsymbol{\xi}_t \sim GP(\mathbf{0}, \boldsymbol{\Sigma}_z) \quad (10)$$

The set of knots were placed using the function `makegrid` from the R package `sp` (Pebesma and Bivand, 2005). A regular grid with approximately 100 points was initially created across the study area, and only the points that fell inside the study boundaries were retained, resulting in a total of 104 knots. The implementation of the GPP model used for comparison is available in the R package `spTimer` (Bakar and Sahu, 2015).

Table 4: Comparison of performance between the proposed NNGP model and another scalable model for large spatiotemporal data (GPP).

Model	Coverage		CRPS	RMSE			MAE		
	95%	90%		space	space-time	time	space	space-time	time
NNGP	95.1	93.3	1.66	0.22	0.17	0.12	0.15	0.14	0.09
GPP	95.8	93.9	2.71	0.31	0.27	0.25	0.22	0.23	0.21

The results of model comparison between the proposed model (NNGP) and the competitor scalable spatiotemporal model (GPP) are presented in Table 4. The proposed model demonstrated lower error in terms of RMSE and MAE for the three predictive scenarios, including unobserved locations at observed times, monitoring stations at future times and unobserved locations at future times. Specifically, the NNGP model has greater predictive accuracy in both spatial and temporal extrapolations. Additionally, the NNGP exhibited lower CRPS values, which reflect narrower and more reliable prediction intervals and achieved better coverage closer to ideal values. These findings highlight that the NNGP outperforms the GPP model both in predictive accuracy and uncertainty quantification, making it a more effective approach for addressing large-scale spatiotemporal hydrological problems.

## 5.2 Comparison with a single-basin model

In this section, we investigate the advantages of the proposed model by comparing it to models that focus on a single basin, a common approach in hydrology (Varouchakis et al., 2022; Varouchakis and Hristopoulos, 2019; Kazemi et al., 2021; Ruybal et al., 2019). Single-basin models are convenient because they alleviate the computational bottleneck of inverting large covariance matrices while preserving the unique characteristics of the basin. However, they may limit the model’s ability to leverage information from multiple basins, which could enhance its performance. Our comparison aims to highlight the trade-off between computational feasibility and model robustness when scaling to larger, multi-basin datasets.

A secondary objective of this comparison is to investigate the benefits of incorporating the autoregressive process into the dependent variable, as proposed in this work (Equations 6 and 7) compared to embedding it within the spatial process (Equations 9 and 10). While both models capture the spatial dependence, they use different approaches - using nearest neighbors to condition each location to small conditional sets for each location (NNGP) and applying dimension reduction followed by kriging (GPP) - which may lead to an unfair comparison when investigating the placement of the autoregressive component. To ensure a more balanced evaluation, we instead model the spatial process assuming a standard GP prior in both formulations. These models are presented in Equations 11 and 12. This comparison allows us to assess how the placement of the autoregressive component affects a model when dealing with spatiotemporal data collected over extended period of time.

In terms of the basin district to be analysed, the Shannon basin was selected for the single-basin models due to its hydrological importance, covering approximately one fifth of Ireland’s land area (see Figure 12). Based on the training and validation split outlined in Section 4, we selected the stations within Shannon, yielding 94 stations for training and 7 for validation. To enable a direct comparison between the the proposed model and single-basin models, the performance was evaluated exclusively at these stations within the Shannon.

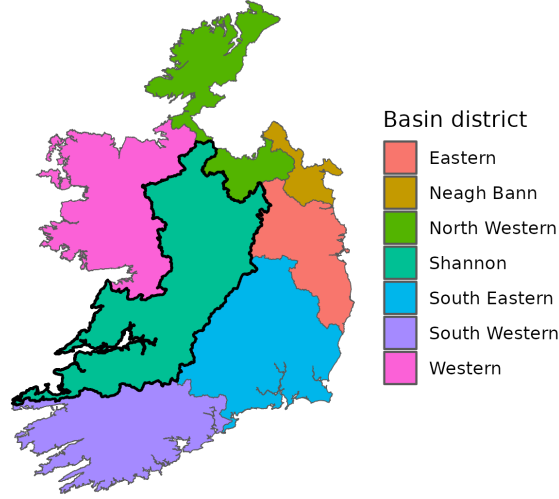


Figure 12: River basin districts of Ireland and the Shannon basin boundaries highlighted in black chosen as reference basin for comparison with single-basin models.

### 5.2.1 GP 1: Autoregressive process into the dependent variable

Spatiotemporal GP model that the mean at current time depends on the response in the previous time.

$$\begin{aligned}
 p(\mathbf{y}_t \mid \mathbf{y}_{t-1}, \mathbf{X}_t, \mathbf{X}_{t-1}, \boldsymbol{\theta}) &\sim \mathcal{N}(\mathbf{y}_t; \boldsymbol{\mu}_t, \boldsymbol{\Sigma} + \tau^2 \mathbf{I}) \\
 \boldsymbol{\mu}_t &= \mathbf{X}_t \boldsymbol{\beta} + \phi(\mathbf{y}_{t-1} - \mathbf{X}_{t-1} \boldsymbol{\beta}).
 \end{aligned} \tag{11}$$

### GP 2: Autoregressive process within the spatial process

Spatiotemporal GP model that the temporal dependence is incorporated in the spatial process.

$$\begin{aligned}
 p(\mathbf{y}_t \mid \mathbf{X}_t, \mathbf{z}_t, \boldsymbol{\theta}) &\sim \mathcal{N}(\mathbf{y}_t; \mathbf{X}_t \boldsymbol{\beta} + \mathbf{w}_t, \tau^2 \mathbf{I}) \\
 \mathbf{w}_t &= \rho \mathbf{w}_{t-1} + \boldsymbol{\xi}_t, \quad \boldsymbol{\xi}_t \sim GP(\mathbf{0}, \boldsymbol{\Sigma}).
 \end{aligned} \tag{12}$$

Table 5: Comparison of performance between the proposed NNGP model and single-basin models (GP 1 and GP 2).

Model	Coverage		CRPS	RMSE			MAE		
	95%	90%		space	space-time	time	space	space-time	time
NNGP	95.81	93.97	1.40	0.18	0.16	0.14	0.12	0.14	0.10
GP 1	95.76	94.17	0.99	0.18	0.15	0.12	0.12	0.13	0.08
GP 2	98.52	98.02	1.50	0.26	0.12	0.16	0.20	0.10	0.13

The results of model comparison between the proposed NNGP model, which uses multi-basin data and the single-basin models GP 1 and GP 2 are shown in Table 5. Comparing the two GP models, the GP 1 model exhibits substantially lower RMSE and MAE compared to GP 2 when partial historical information is available for the observation to be predicted - either at unobserved locations with observed times or at monitoring stations projecting into future time points. However, in the absence of such historical data, a scenario that requires extrapolation across both space and time, the GP 2 model performs better in terms of both error metrics. This suggests that incorporating the autoregressive process into the spatial latent field (as in GP 2) provides a more effective mechanism for capturing the latent spatiotemporal dynamics when historical observations are unavailable. These findings highlight the strengths of each model depending on the predictive scenario, with GP 1 better suited for cases where the prediction is purely spatial or temporal. While, GP 2 excelling in capturing latent spatial-temporal dependencies when data is more limited.

In terms of the uncertainty estimation, the GP 1 model showed smaller CRPS compared to GP 2, indicating that the prediction intervals are narrower and more concentrated around the observed values. Additionally, the posterior predictive distribution for GP 2 is more dispersed as shown by the higher coverage values above the nominal level. These results suggest that incorporating the autoregressive process into the dependent variable (as in GP 1 and in the

---

proposed NNGP model) is more appropriate for capturing temporal dependencies in long-term spatiotemporal datasets. Moreover, in that formulation, the autoregressive parameter offers a more natural interpretation, as it is directly tied to the response variable, specifically quantifying the degree of dependence between water levels on successive days.

When compared the performance between the proposed NNGP model and the GP 1 model, which has the same formulation but assumes a GP prior for the spatial latent field, the single-basin GP 1 model exhibited slightly superior predictive accuracy. While the GP 1 model achieved marginally lower RMSE and MAE values, the differences were not substantial. In terms of uncertainty quantification, the 95% coverage for both NNGP and GP 1 models were close to the ideal level, while the 90% coverage for all the models exceeded the target. However, the NNGP model's coverage was slightly closer to the desired level, indicating it provides more reliable uncertainty estimates. This is particularly important for hydrological applications where the range of the predicted water level is crucial for risk assessment and decision-making.

The results demonstrate that the NNGP approximation exhibits comparable predictive performance to its full GP method. Additionally, the NNGP balances between predictive accuracy and precision. While there is a minimal trade-off in performance compared to the single-basin model, GP 1, the key advantage of the NNGP lies in its scalability and its ability to extend predictions across a broader range of river basins, making it more versatile for large-scale hydrological applications.

## 6 Limitations

This work proposes a model for predicting water level on rivers in Ireland considering a long-term spatiotemporal data. This approach has been demonstrated to be effective, as evidenced by the promising results. However, several limitations should be noted. As previously mentioned, the model incorporates only precipitation as a predictor. The inclusion of additional hydroclimate predictors such as temperature, wind speed, soil moisture and potential evapotranspiration would potentially improve the predictive performance and reliability of the model. Additionally, the misalignment problem between the hydroclimate factors, and the water level was addressed through Inverse Distance Weighting interpolation. Despite the simplicity and efficacy of this methodology, a complex probabilistic interpolation approach could be investigated to potentially enhance the precision of estimations. However, the development of such techniques falls beyond the scope of this study.

In the proposed model, the spatial dependence is captured through a spatial latent field specified as a NNGP, which fundamentally depends on the covariance structure. The introduced structure is straightforward and effective, ensuring computational feasibility without compromising performance. However, it simplifies the complex spatial dependencies inherent in river networks, where flow directionality and confluences may impact the water level measurements along the river. Addressing this limitation could involve specifying a more sophisticated covariance structure that accounts for the distance along the river network and flow directionality. Such covariance structures combined with NNGP are not present in the literature, as far as we are aware, and therefore we view this as a future research direction.

## 7 Conclusion

In this paper, we proposed a spatiotemporal NNGP model for predicting water level in a long-term dataset across both space and time. This model not only delivers accurate predictions but also quantifies uncertainty for both monitored stations and unobserved locations. By accounting for spatiotemporal dependencies and incorporating precipitation information, the model offers insights of the impact of precipitation on water levels over time, thereby supporting more informed decision-making in hydrological monitoring, early warning systems, and adaptive resource planning.

We compared our approach with the GPP model, a competitor model for large spatiotemporal data well known in the literature. The proposed model demonstrated superior performance in terms of prediction accuracy and a higher degree of confidence its estimations. Furthermore, we also compared our proposed model with approaches encountered in the field of hydrology. Typically, these approaches rely on GP models for a single basin, thus, avoiding the computational limitations of inversions of large covariance matrices. Despite the minimal loss in performance, the NNGP offers the advantage of handling a large number of spatial points across multiple basins. This scalability enables broader application to large-scale river networks, extending prediction capabilities across a wider range of river basins, and capturing the interconnected spatial dependencies within hydrological systems.

Furthermore, our findings demonstrated that for large spatiotemporal datasets with observations collected over an extended period, the specification of the time component in the proposed model enhances the predictive accuracy in scenarios focused exclusively on spatial or temporal predictions. The advantages of the specified temporal component were also observed in the precision of the estimations, with the predictions closer to the true values and narrower

---

prediction intervals. This finding indicates that the given specification of the temporal component is a crucial factor in the successful solution to the given hydrological problem.

Despite the importance of the specification of a temporal parameter, the key component of our model is the inclusion of a NNGP spatiotemporal latent field. The NNGP overcomes the computational challenges of a traditional GP when analysing a large dataset. While the methodology is still under active research, this work introduces a novelty in the application of the NNGP specifically for predicting water levels in river networks. Moreover, existing models in the hydrology literature have not explored a Bayesian statistical model accounting for a large dataset that span both spatial and temporal dimensions.

## 8 Acknowledgments

This publication has emanated from research conducted with the financial support of Science Foundation Ireland under Grant number 18/CRT/6049.

## References

- Abdulah, S., Alamri, F., Nag, P., Sun, Y., Ltaief, H., Keyes, D. E., and Genton, M. G. (2022). The second competition on spatial statistics for large datasets. *Journal of Data Science*, 20(4):439–460.
- Ahmed, A. N., Yafouz, A., Birima, A. H., Kisi, O., Huang, Y. F., Sherif, M., Sefelnasr, A., and El-Shafie, A. (2022). Water level prediction using various machine learning algorithms: a case study of durian tunggal river, malaysia. *Engineering Applications of Computational Fluid Mechanics*, 16:422–440.
- Bakar, K. S. and Sahu, S. K. (2015). spTIMER: Spatio-temporal bayesian modeling using R. *Journal of Statistical Software*, 63(15):1–32.
- Charlton, R., Fealy, R., Moore, S., Sweeney, J., and Murphy, C. (2006). Assessing the impact of climate change on water supply and flood hazard in ireland using statistical downscaling and hydrological modelling techniques. *Climatic Change*, 74:475–491.
- Chen, F. W. and Liu, C. W. (2012). Estimation of the spatial rainfall distribution using inverse distance weighting (IDW) in the middle of taiwan. *Paddy and Water Environment*, 10:209–222.
- Datta, A., Banerjee, S., Finley, A. O., and Gelfand, A. E. (2016a). Hierarchical nearest-neighbor gaussian process models for large geostatistical datasets. *Journal of the American Statistical Association*, 111:800–812.
- Datta, A., Banerjee, S., Finley, A. O., Hamm, N. A., and Schaap, M. (2016b). Nonseparable dynamic nearest neighbor gaussian process models for large spatio-temporal data with an application to particulate matter analysis. *Annals of Applied Statistics*, 10:1286–1316.
- Finley, A. O., Datta, A., Cook, B. D., Morton, D. C., Andersen, H. E., and Banerjee, S. (2019). Efficient algorithms for bayesian nearest neighbor gaussian processes. *Journal of Computational and Graphical Statistics*, 28(2):401–414. PMID: 31543693.
- Gabry, J., Češnovar, R., Johnson, A., and Bröder, S. (2024). *cmdstanr: R Interface to 'CmdStan'*. R package version 0.8.1, <https://discourse.mc-stan.org>.
- Gneiting, T. and Raftery, A. E. (2007). Strictly proper scoring rules, prediction, and estimation. *Journal of the American Statistical Association*, 102:359–378.
- Hoogland, T., Heuvelink, G. B., and Knotters, M. (2010). Mapping water-table depths over time to assess desiccation of groundwater-dependent ecosystems in the netherlands. *Wetlands*, 30:137–147.
- Júnez-Ferreira, H. E. and Herrera, G. S. (2013). A geostatistical methodology for the optimal design of space-time hydraulic head monitoring networks and its application to the valle de querétaro aquifer. *Environmental Monitoring and Assessment*, 185:3527–3549.
- Kazemi, H., Sarukkalige, R., and Shao, Q. (2021). Evaluation of non-uniform groundwater level data using spatiotemporal modeling. *Groundwater for Sustainable Development*, 15.
- Kenda, K., Peternelj, J., Mellios, N., Kofinas, D., Čerin, M., and Rožanec, J. (2020). Usage of statistical modeling techniques in surface and groundwater level prediction. *Journal of Water Supply: Research and Technology - AQUA*, 69:248–265.
- Marie (2023). Met Éireann data api. <https://marie.ie/repo/met-eireann-api/>. last access: 28 November 2023.

- 
- Mastrantonio, G., Lasinio, G. J., Pollice, A., Capotorti, G., Teodonio, L., Genova, G., and Blasi, C. (2019). A hierarchical multivariate spatio-temporal model for clustered climate data with annual cycles. *Annals of Applied Statistics*, 13:797–823.
- Molinos, J. G., Viana, M., Brennan, M., and Donohue, I. (2015). Importance of long-term cycles for predicting water level dynamics in natural lakes. *PLoS ONE*, 10.
- Murphy, C., Coen, A., Clancy, I., Decristoforo, V., Cathal, S., Healion, K., Horvath, C., Jessop, C., Kennedy, S., Lavery, R., Leonard, K., McLoughlin, C., Moore, R., O’Hare-Doherty, D., Paisley, R., Prakash, B., Vatu, J., Thorne, P., Mateus, C., Ryan, C., and Noone, S. (2023). The emergence of a climate change signal in long-term irish meteorological observations. *Weather and Climate Extremes*, 42.
- OPW (2021). Real-time water level data. <https://waterlevel.ie/>. last access: 28 November 2023.
- Pagendam, D., Janardhanan, S., Dabrowski, J., and MacKinlay, D. (2023). A log-additive neural model for spatio-temporal prediction of groundwater levels. *Spatial Statistics*, 55.
- Pan, M., Zhou, H., Cao, J., Liu, Y., Hao, J., Li, S., and Chen, C. H. (2020). Water level prediction model based on gru and cnn. *IEEE Access*, 8:60090–60100.
- Pebesma, E. J. and Bivand, R. (2005). Classes and methods for spatial data in R. *R News*, 5(2):9–13.
- Ruybal, C. J., Hogue, T. S., and McCray, J. E. (2019). Evaluation of groundwater levels in the arapahoe aquifer using spatiotemporal regression kriging. *Water Resources Research*, 55:2820–2837.
- Sahu, S. K. and Bakar, K. S. (2012). Hierarchical bayesian autoregressive models for large space–time data with applications to ozone concentration modelling. *Applied Stochastic Models in Business and Industry*, 28(5):395–415.
- Santos-Fernandez, E., Hoef, J. M. V., Peterson, E. E., McGree, J., Isaak, D. J., and Mengersen, K. (2022). Bayesian spatio-temporal models for stream networks. *Computational Statistics and Data Analysis*, 170.
- van der Knijff, J. M., Younis, J., and de Roo, A. P. (2010). Lisflood: A gis-based distributed model for river basin scale water balance and flood simulation. *International Journal of Geographical Information Science*, 24:189–212.
- Varouchakis, E. A., Guardiola-Albert, C., and Karatzas, G. P. (2022). Spatiotemporal geostatistical analysis of groundwater level in aquifer systems of complex hydrogeology. *Water Resources Research*, 58.
- Varouchakis, E. A. and Hristopulos, D. T. (2019). Comparison of spatiotemporal variogram functions based on a sparse dataset of groundwater level variations. *Spatial Statistics*, 34.
- Vecchia, A. V. (1988). Estimation and model identification for continuous spatial processes. *Journal of the Royal Statistical Society: Series B (Methodological)*, 50(2):297–312.
- Willner, S. N., Otto, C., and Levermann, A. (2018). Global economic response to river floods. *Nature Climate Change*, 8:594–598.